

ELECTRON BACKSCATTER DIFFRACTION (EBSD) OF SHERGOTTITES NORTHWEST AFRICA (NWA) 15628, NWA 12241, AND DHOFAR (DHO) 019. G. A. Anim¹ and A. M. Ruzicka¹, ¹Cascadia Meteorite Laboratory (ganim@pdx.edu), Portland State University, Department of Geology, Portland, OR 97207, USA.

Introduction: Until samples can be returned from Mars by spacecraft [1], martian meteorites are the only samples we currently can study in laboratories on Earth. Martian meteorites identified so far are predominantly shergottites, which are basaltic in composition, similar to terrestrial basalts [2,3]. Their mineralogy is predominantly pigeonite, augite, plagioclase (mostly amorphized into an isotropic glass called maskelynite), and sometimes olivine.

Since these rocks are separated from the martian surface by strong impact events on Mars [4,5], they are overprinted by intense shock metamorphism. Shock metamorphism is the range of effects produced when two heavenly bodies collide [6]. Shock metamorphism intensity can be estimated using the shock stage [7] and weighted shock stage [8] classifications, which are based on observed shock metamorphic features under the optical microscope.

Newer Scanning Electron Microscope – Electron Backscatter Diffraction (SEM-EBSD) methods have been developed which use the plastic deformation in mineral grains to quantify the overall deformation experienced by the sample [9]. An EBSD metric known as Grain Orientation Spread (GOS), which measures the average misorientation within a grain, is very robust for measuring overall deformation, and mean GOS is highly correlated with weighted shock stage [9]. Also, optical shock stage is somewhat imprecise [10] and ultimately somewhat qualitative, whereas GOS is precise, quantitative, and can be determined for a statistically large number of different mineral grains. Here, we evaluate shock effects in three shergottites: Northwest Africa (NWA) 15628, NWA 12241 and Dhofar (Dho) 019 using both standard optical petrography as well as SEM-EBSD and energy dispersive spectroscopy (EDS) methods.

Methods and Samples: A Leica DM2500 petrographic microscope was used to study the petrography and shock stages [7] of one thin section from each meteorite. The thin sections were further hand polished using colloidal silica in 20-minute increments for a total of ~60-61 minutes. The samples were then coated with an ~3-5 nm carbon coat for SEM-EBSD analysis. A Zeiss Sigma Variable Pressure-Field Emission Gun-Scanning Electron Microscope (VP-FEG-SEM) was used for EBSD analysis at Portland State University. Acquired data were processed using Oxford Instruments Aztec and AztecCrystal software.

The mean GOS values for olivine, pigeonite, and augite were determined for different grain size ranges because GOS depends on grain size [9]. GOS values of grains with equivalent circle diameter $>50\mu\text{m}$ (designated as $\text{GOS}_{d>50}$) are used because they correlate strongly with shock stage estimates [9]. In this abstract we combine data for pigeonite and augite as “pyroxene”.

Results:

NWA 12241. This is a poikilitic shergottite with olivine, pyroxene, birefringent plagioclase, and amorphous plagioclase [11]. Plagioclase-composition glass is not considered to be maskelynite [11,12]. However, the composition of this glass and its textural appearance is identical to maskelynite found in other shergottites. Also we found mixing between isotropic plagioclase glass and shock melt pockets (average size = $0.13\pm 0.05\text{mm}$) similar to [13] (Figure 1). This suggests the existence of maskelynite in NWA 12241. The interface between melt pockets and maskelynite have crystallites of a new phase which could be either tissantite or stöfflerite. Shock stage is judged to be low (M-S3) [12].

Olivine grains have a mean $\text{GOS}_{d>50}$ of $3.46\pm 1.49^\circ$ ($N_g = \text{number of grains} = 944$). Pyroxene grains have a mean $\text{GOS}_{d>50}$ value of $2.70\pm 1.06^\circ$ ($N_g=384$). In both olivine and pyroxene, there is a small population of high-GOS grains.

Dho 019. This is a doleritic rock consisting of pyroxene, zoned olivine megacrysts and fully converted maskelynite. It has shock features consistent with a shock stage of M-S4 but melt pockets are relatively rare [15]. This suggests lower pressures and temperatures (P-T) during shock.

Olivine grains have a mean $\text{GOS}_{d>50}$ value of $3.75\pm 1.4^\circ$ ($N_g = 333$). Furthermore $\text{GOS}_{d>50}$ olivine statistics (Figure 2) show a bimodal distribution. Pyroxene grains have a mean $\text{GOS}_{d>50}$ value of $2.16\pm 1.06^\circ$ ($N_g = 1806$). There is a small portion of olivine grains with higher GOS values (up to $\sim 10^\circ$).

NWA 15628. This is a basaltic shergottite dominated by pyroxene and maskelynite. It has a shock stage of M-S4 [14]. Though it has the same shock stage as Dho 019, the size of melt pockets and intensity of fracturing suggests it may have experienced higher P-T during shock.

Pyroxene grains in this meteorite have a mean $GOS_{d>50}$ value of $4.70 \pm 1.09^\circ$ ($N_g = 216$). The pyroxene GOS chart (Figure 3) shows a weak bimodality.

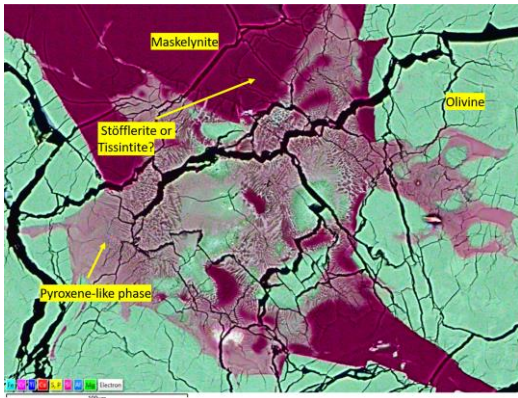


Figure 1: False color energy dispersive spectroscopy (EDS) map of melt pocket in NWA 12241. Phases are maskelynite (dark purple), olivine (green), pyroxene-like phase (light purple) and suspected tissintite or stöfflerite phase (dark purple adjacent maskelynite).

Discussion: Mean olivine $GOS_{d>50}$ values are slightly higher in Dho 019 ($3.75 \pm 1.4^\circ$) than in NWA 12241 ($3.46 \pm 1.49^\circ$) consistent with the shock stages as predicted by [9]. The closeness of the $GOS_{d>50}$ values for both suggest that Dho 019 might be a lower M-S4 shock stage and NWA 12241 might be a higher M-S3. This is confirmed by the shock features in Dho 019 [15] and NWA 12241 (this work and [11]). The bimodal distribution of olivine GOS in Dho 019 suggests an earlier deformation history that was not recorded by pyroxene. There are no olivine grains in NWA 15628 so it could not be compared.

Values for mean $GOS_{d>50}$ in pyroxene are generally lower than in olivine. Contrary to the olivine trend, pyroxene in NWA 12241 has a higher mean $GOS_{d>50}$ ($2.70 \pm 1.06^\circ$) than Dho 019 ($2.16 \pm 1.06^\circ$) for reasons that are yet unclear. NWA 15628 has the highest mean $GOS_{d>50}$ ($4.70 \pm 1.09^\circ$) which is consistent with its higher shock stage. In NWA 15628, the weak GOS bimodality in pyroxene could signify two deformation events analogous to that shown by olivine in Dho 019.

GOS bimodality could be caused by proximity of grains to high P-T areas such as shock veins and melt pockets but this seems unlikely. This is because NWA 12241 has a shock vein but no bimodality, Dho 019 had a small shock melt pocket yet had the strongest bimodality, and the portion analysed in NWA 15628 had no shock melts or veins yet was weakly bimodal.

We speculate that the prevalent GOS peak in the bimodal GOS charts was produced by the final impact event that ejected the meteorites. The other peak may represent a relatively strong deformation event (be-

cause of the high GOS). The nature of this earlier deformation is uncertain but could be impact, magmatic deformation, deformation associated with mantle convection or with rapid ascent of crystal-bearing magmas.

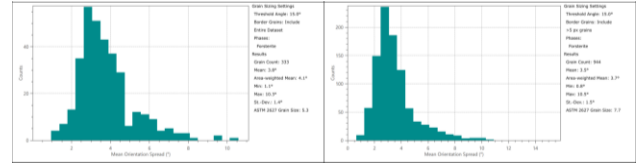


Figure 2: Mean Grain Orientation Spread for Olivine grains $>50\mu m$ in Dho 019 (left) and NWA 12241 (right). Notice the bimodality in Dho 019.

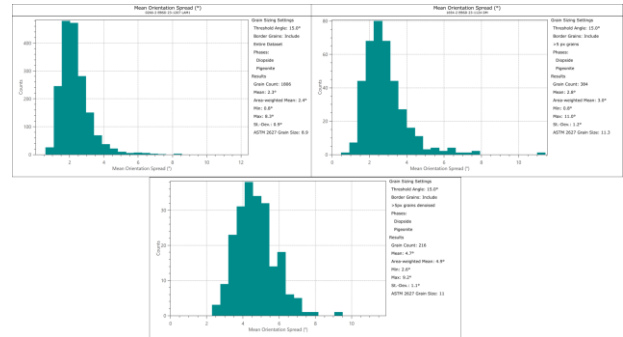


Figure 3: Mean Grain Orientation Spread for pyroxene grains $50\mu m$ in Dho 019 (left), NWA 12241 (right) and NWA 15628 (bottom). Notice the weak bimodality in NWA 15628.

Acknowledgments: This research was funded by the Barringer Family Fund and Sigma Xi Grants in aid of research (G20230315-5130).

This work would not have been possible if not for the guidance of Alexander Ruzicka and Daniel Sheikh.

References: [1] Udry et al (2020) *J. Geophys. Res. Planets*. [2] Kizovski et al (2019) *MaPS*, **54**, 768–784. [3] McSween (2015) *Am. Min.*, **100**, 2380–2395. [4] Artemieva and Ivanov (2004) *Icarus*, 171, pp. 84–101 [5] Fritz et al (2005) *MaPS*, **40**, 1393–1411. [6] DeCarli (2005) in *Encycl of Geol*, 179–184. [7] Stöffler et al (2018) *MaPS*, **53**, 5–49, 2018. [8] Jamsja and Ruzicka (2010), *MaPS*, **45**, 828–849, [9] Ruzicka and Hugo (2018) *Geochimica et Cosmochimica Acta*, **234**, 115–147. [10] Stöffler (1991) *Geochimica et Cosmochimica Acta*, **55**, 3845–3867. [11] A. Udry et al. (2021), *LPSC 52*, Abstract # 2548. [12] Lapen et al. (2019) *LPSC 50* Abstract # 2132. [13] El Goresy et al. (2013), *Geochimica et Cosmochimica Acta*, **101**, 233–262. [14] *Met. Bull. Database*, <https://www.lpi.usra.edu/meteor/metbull.php>. [15] *Martian Meteorite Compendium* <https://www-curator.jsc.nasa.gov/antmet/mmc/>.